Models of fracture of cellular monolith structures

Y.A.Antipov[1], A.B.Movchan[2], S.T.Kolaczkowski[3]

[1]Department of Mathematical Sciences, University of Bath
Claverton Down, Bath BA2 7AY, UK, E-mail: masya@maths.bath.ac.uk
[2]Department of Mathematical Sciences, The University of Liverpool
Liverpool L69 3BX, UK
[3]Department of Chemical Engineering, University of Bath
Claverton Down, Bath BA2 7AY, UK

Abstract

This work deals with homogenization models for cracks in lattice structures representing cross-sections of catalytic monolith combustors. An asymptotic approach is used to describe interaction of cracks and to evaluate the stress-intensity factors. A comparison is given for a critical load evaluated on the basis of the homogenization model and a critical load obtained from the experiment. An accurate asymptotic model of local stability of a crack interacting with a micro-defect is presented.

1 Introduction

A catalytic combustor is represented by a ceramic cellular monolith structure with square, hexagonal or triangular cells. For description of combustion reactions in a catalytic monolith we refer to Hayes and Kolaczkowski (1997). In the present paper we are mainly concerned with elastic fields in a damaged lattice structure. The homogenization models for cellular structures with square cells were studied in Antipov et al (1999) with applications to propagation of cracks and crack-defect interaction. A particular feature of the lattice structure with square cells is a low resistance to shear; the homogenized material is orthotropic. In the present paper we consider two remaining possibilities: hexagonal and triangular lattice structures. In both cases, the homogenization procedure gives isotropic media; however, the hexagonal structure is characterized by a small shear modulus (see Gibson and Ashby (1988)). It is appropriate to refer to the work by Hori and Nemat-Nasser (1987) and Gong and Horii (1989) who studied numerically a long-range interaction between a finite crack and a micro-crack in 2D isotropic media. The results of the present paper are mainly analytical; the dipole fields associated with a small micro-crack were evaluated explicitly, and the asymptotic algorithm described below is similar to the one employed in the earlier work of Antipov et al (1999). The main results include:

(1) asymptotic formulae for the stress-intensity factors associated with crack-defect interaction in hexagonal and triangular lattice structure;

(2) comparison of asymptotic estimates for the stress-intensity factors for different lattice geometries;

(3) local stability analysis in crack-defect interaction;

(4) comparison of the homogenization results with the analysis of the lattice structures.

The structure of the paper can be described as follows. In Section 2 we give formulation of the problem that includes governing equations, boundary conditions, characteristics of the homogenized elastic media with cracks. In section 3 we give explicit description of dipole fields for cracks. Section 4 includes the outline of the asymptotic algorithm used for evaluation of the stress intensity factors. We consider the particular case of thermal load in Section 5. Section 6 presents numerical results for the stress intensity factors and the local stability analysis for the crack-defect interaction. Appendix compares the critical temperature (required to initiate fracture) associated with the homogenization model and the critical temperature obtained from the experiment for the case of a lattice structure with square cells.

2 Governing equations and homogenization

We consider two types of lattice structures (with hexagonal or triangular cells), where the homogenized two-dimensional elastic material is isotropic, i.e. the averaged displacement field $\mathbf{u}$ satisfies the system of equilibrium equations

$$\mu_* \nabla^2 \mathbf{u} + (\lambda_* + \mu_*) \nabla \nabla \cdot \mathbf{u} = 0, \tag{2.1}$$

where λ_* and μ_* are the 2D Lamé elastic moduli of the homogenized material. The equivalent representation of (2.1) is given by

$$\boldsymbol{\mathcal{D}}^T \left(\frac{\partial}{\partial x} \right) \boldsymbol{\mathcal{H}} \boldsymbol{\mathcal{D}} \left(\frac{\partial}{\partial x} \right) \mathbf{u} = 0 \tag{2.2}$$

where $\boldsymbol{\mathcal{H}}$ is 3×3 matrix of the 2D elastic moduli of the homogenized material, and the differential operator $\boldsymbol{\mathcal{D}}$ has the form

$$\boldsymbol{\mathcal{D}} \left(\frac{\partial}{\partial x} \right) = \begin{pmatrix} \frac{\partial}{\partial x_1} & 0 \\ 0 & \frac{\partial}{\partial x_2} \\ \frac{1}{\sqrt{2}} \frac{\partial}{\partial x_2} & \frac{1}{\sqrt{2}} \frac{\partial}{\partial x_1} \end{pmatrix}. \tag{2.3}$$

For triangular and hexagonal lattice structures (see Fig. 1) the matrices of homogenized elastic moduli are defined as

$$\boldsymbol{\mathcal{H}}^{triang} = \frac{E}{1-\nu^2} \begin{pmatrix} \frac{3}{8} f & \frac{1}{8} f & 0 \\ \frac{1}{8} f & \frac{3}{8} f & 0 \\ 0 & 0 & \frac{1}{4} f \end{pmatrix}, \tag{2.4}$$

and

$$\boldsymbol{\mathcal{H}}^{hexag} = \frac{E}{1-\nu^2} \begin{pmatrix} \frac{1}{4} f + \frac{3}{8} f^3 & \frac{1}{4} f - \frac{3}{8} f^3 & 0 \\ \frac{1}{4} f - \frac{3}{8} f^3 & \frac{1}{4} f + \frac{3}{8} f^3 & 0 \\ 0 & 0 & \frac{3}{4} f^3 \end{pmatrix}. \tag{2.5}$$

where f is the area fraction of the elastic material in the 2D lattice, and E, ν are the Young modulus and the Poisson ratio of the elastic material (derivation of (2.4) and (2.5) is given in Kolaczkowski et al (1999)). It follows from (2.4), (2.5) that the coefficients λ_*, μ_* in (2.1) are

$$\lambda_* = \mu_* = \frac{f}{8} \frac{E}{1-\nu^2} \tag{2.6}$$

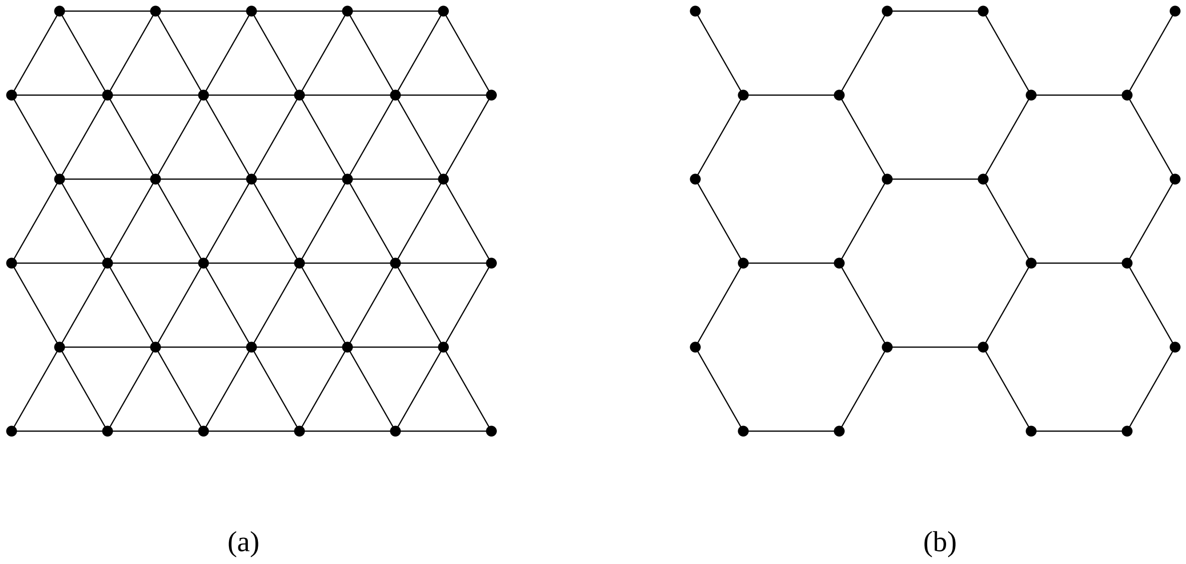

Figure 1: Lattice structures

for the case of triangular lattice, and

$$\lambda_* = \frac{f}{4}\left(1 - \frac{3}{2}f^2\right)\frac{E}{1-\nu^2}, \quad \mu_* = \frac{3}{8}f^3\frac{E}{1-\nu^2} \tag{2.7}$$

for hexagonal lattice structures. We remark that in three dimensions the homogenized materials above should be treated as transversely isotropic (their elastic properties in (x_1, x_2)-plane are different from those in (x_1, x_3) and (x_2, x_3) planes).

Let a homogenized 2D medium contain two cracks (see Fig. 2)

$$M = \{\mathbf{x} : |x_1| < a, \, x_2 = 0\}, \tag{2.8}$$

and

$$m_\varepsilon = \{\mathbf{x} : x_j = x_j^{(0)} + l_j t, \quad j = 1, 2, \quad |t| < \varepsilon\}, \tag{2.9}$$

where ε is a small positive non-dimensional parameter, and $a, x_j^{(0)}, l_j$ are given constants: the crack M has a finite length $2a$, and the crack m_ε is small, of the length 2ε; $\mathbf{x}^{(0)} = (x_1^{(0)}, x_2^{(0)})$ and $\mathbf{l} = (l_1, l_2), ||\mathbf{l}|| = 1$, characterize the location and orientation of the small crack. It is also assumed that $\mathbf{x}^{(0)}$ is located at a finite distance from the crack M.

Traction boundary conditions are posed in the homogenized medium for the field $\mathbf{u}$ on the crack faces $M^\pm$ and $m_\varepsilon^\pm$:

$$\boldsymbol{\mathcal{D}}^T(\mathbf{n})\boldsymbol{\mathcal{H}}\boldsymbol{\mathcal{D}}\left(\frac{\partial}{\partial x}\right)\mathbf{u} = \mathbf{p}(\mathbf{x}) \quad \text{on} \quad M^\pm \cup m_\varepsilon^\pm, \tag{2.10}$$

where $\mathbf{n}$ represents the unit normal on the crack faces; the principal force and moment vectors associated with the load $\mathbf{p}$ are assumed to be zero.

We seek the solution $\mathbf{u}$ with finite elastic energy. We shall evaluate the stress-intensity factors for the crack M as functions of position and orientation of the micro-crack m_ε (the stress-intensity factors also depend, of course, on the applied load, but we deal with a model situation when the load density is constant), and analyze the local stability of the crack M.

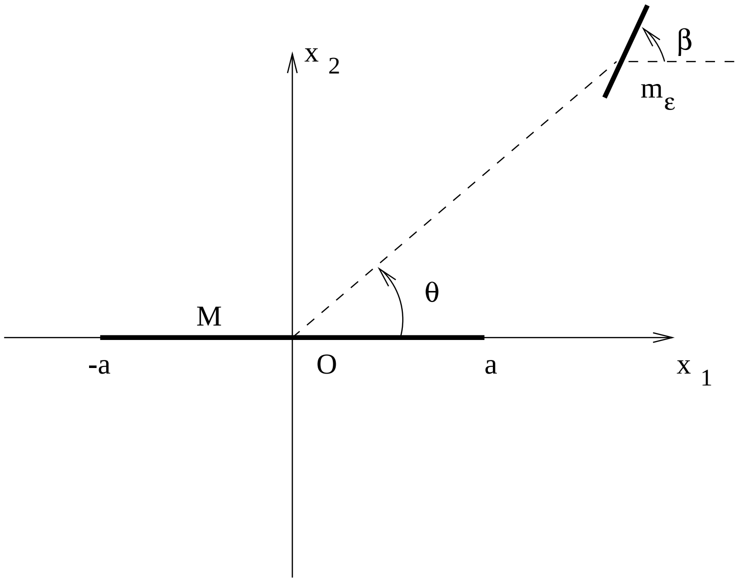

Figure 2: Geometry of the homogenized problem: a macro-crack M and a micro-crack m_ε.

3 Dipole fields for cracks

The asymptotic scheme introduced in the text below involves so-called dipole fields for cracks. Let $\mathfrak{M}$ be a crack of the finite length $2l$ inclined at the angle β to the x_1-axis. One can introduce three model fields in $\mathbb{R}^2 \setminus \mathfrak{M}$

$$\mathbf{U}^{(j)}(\mathbf{x}) = \mathbf{V}^{(j)}(\mathbf{x}) + \mathbf{W}^{(j)}(\mathbf{x}), \quad j = 1, 2, 3, \tag{3.1}$$

which satisfy the homogeneous equilibrium equations, homogeneous traction boundary conditions and grow linearly at infinity. The fields $\mathbf{V}^{(j)}$ are defined by

$$\mathbf{V}^{(1)}(\mathbf{x}) = \begin{pmatrix} x_1 \\ 0 \end{pmatrix}, \quad \mathbf{V}^{(2)}(\mathbf{x}) = \begin{pmatrix} 0 \\ x_2 \end{pmatrix} \quad \text{and} \quad \mathbf{V}^{(3)}(\mathbf{x}) = \frac{1}{\sqrt{2}} \begin{pmatrix} x_2 \\ x_1 \end{pmatrix}, \tag{3.2}$$

and produce constant components of strain. Vector functions $\mathbf{W}^{(j)}$, $j = 1, 2, 3$, are assumed to decay at infinity, and they compensate for the discrepancy left by $\mathbf{V}^{(j)}$ in the traction boundary conditions on the crack faces; $\mathbf{W}^{(j)}$ are called the dipole fields of the crack $\mathfrak{M}$. At infinity, $\mathbf{W}^{(j)}$ have the following asymptotic representation:

$$\mathbf{W}^{(j)} = \sum_{j=1}^{3} P_{jk} \left(\mathbf{V}^{(j)} \left(\frac{\partial}{\partial \mathbf{x}} \right) \right)^T \mathbf{T}(\mathbf{x}) + O\left(\frac{1}{||\mathbf{x}||^2} \right), \tag{3.3}$$

where $\mathbf{V}^{(j)}(\partial/\partial\mathbf{x})$ are the vector differential operators defined by (3.2) (x_j should be replaced by $\partial/\partial x_j$), $\mathbf{T}(\mathbf{x})$ is Green's tensor for 2D elasticity. The matrix $||P_{jk}||_{j,k=1}^3$ is called the dipole matrix of the crack; it is symmetric, negative definite. Explicit representation of the matrix $\mathbf{P}$ (see Movchan and Serkov (1997)) is given by

$$\mathbf{P} = -\frac{\pi l^2(\lambda + 2\mu)}{4\mu} \begin{pmatrix} \Xi + \Omega + \Sigma & \Xi - \Omega & \Lambda \\ \Xi - \Omega & \Xi + \Omega - \Sigma & \Lambda \\ \Lambda & \Lambda & 2\Theta \end{pmatrix}, \tag{3.4}$$

where

$$\Omega = \frac{2\mu^2}{\lambda+\mu}, \quad \Xi = 2(\lambda+\mu), \quad \Sigma = -4\mu\cos 2\beta,$$
$$\Lambda = -2\sqrt{2}\mu\sin 2\beta, \quad \Theta = \mu,$$

and λ, μ are the 2D elastic moduli of the material (compare with (2.1)).

It is straightforward to evaluate the stress components associated with the dipole fields. Assume, for simplicity, that the crack faces are subjected to constant normal and tangential tractions

$$\sigma_{nn} = -p_2^\circ, \quad \sigma_{ns} = -p_1^\circ \tag{3.5}$$

on the crack boundary. Then it follows from (3.3), (3.4) that the stress components are characterized by the following asymptotics:

$$\boldsymbol{\sigma}(\xi_1,\xi_2) = \boldsymbol{\Sigma}(\xi_1,\xi_2) + O(r^{-3}), \quad r\to\infty, \tag{3.6}$$

$$\Sigma_{11}(\xi_1,\xi_2) = \frac{l^2}{2r^2}[-\sin 2\alpha(2\cos 2\alpha+1)p_1^\circ + (2\cos^2 2\alpha - 1)p_2^\circ],$$
$$\Sigma_{12}(\xi_1,\xi_2) = \frac{l^2}{2r^2}[(2\cos^2 2\alpha - 1)p_1^\circ + \sin 2\alpha(2\cos 2\alpha - 1)p_2^\circ],$$
$$\Sigma_{22}(\xi_1,\xi_2) = \frac{l^2}{2r^2}[\sin 2\alpha(2\cos 2\alpha - 1)p_1^\circ + (-2\cos^2 2\alpha + 2\cos 2\alpha + 1)p_2^\circ], \tag{3.7}$$

where polar coordinates (r,α) and the components $\Sigma_{ij}(\xi_1,\xi_2)$ are associated with the local system coordinates (ξ_1,ξ_2) (the ξ_1-axis is aligned along $\mathfrak{M}$) and

$$r = \sqrt{\xi_1^2+\xi_2^2}, \quad \sin 2\alpha = \frac{2\xi_1\xi_2}{r^2}, \quad \cos 2\alpha = \frac{\xi_1^2-\xi^2}{r^2}.$$

4 The asymptotic algorithm

The asymptotic approximation of the displacement field $\mathbf{u}$ is sought in the form

$$\mathbf{u}(\mathbf{x},\varepsilon,f) \sim \mathbf{v}(\mathbf{x},f) + \varepsilon\mathbf{w}(\boldsymbol{\zeta},f) + \varepsilon^2\mathbf{q}(\mathbf{x},f), \tag{4.1}$$

where $\boldsymbol{\zeta} = \varepsilon^{-1}(\mathbf{x}-\mathbf{x}^{(0)})$ defines stretched coordinates introduced in a neighbourhood of the small crack m_ε; f is a small area fraction of material in a 2D lattice; ε is a non-dimensional small parameter characterising the length of m_ε. Here we assume that $\varepsilon << f$.

1. The vector-function $\mathbf{v}$ represents the displacement field in $\mathbb{R}^2\setminus M$. It satisfies the system of equilibrium equations (the micro-crack m_ε is absent). The representation for the field $\mathbf{v}$ is well-known (see Sedov, 1972). The stress components evaluated at $(x_1^{(0)}, x_2^{(0)})$ admit the integral representations:

$$\sigma_{11}^\circ = \frac{1}{\pi}\int_{-a}^{a}\phi_1(\xi)\frac{x_2[3(x_1-\xi)^2+x_2^2]}{[(x_1-\xi)^2+x_2^2]^2}d\xi - \frac{1}{\pi}\int_{-a}^{a}\phi_2(\xi)\frac{(x_1-\xi)[(x_1-\xi)^2-x_2^2]}{[(x_1-\xi)^2+x_2^2]^2}d\xi,$$

$$\sigma_{12}^\circ = -\frac{1}{\pi}\int_{-a}^{a}\phi_1(\xi)\frac{(x_1-\xi)[(x_1-\xi)^2-x_2^2]}{[(x_1-\xi)^2+x_2^2]^2}d\xi + \frac{1}{\pi}\int_{-a}^{a}\phi_2(\xi)\frac{x_2[-(x_1-\xi)^2+x_2^2]}{[(x_1-\xi)^2+x_2^2]^2}d\xi,$$

$$\sigma^{\circ}_{22} = \frac{1}{\pi}\int\limits_{-a}^{a}\phi_1(\xi)\frac{x_2[-(x_1-\xi)^2+x_2^2]}{[(x_1-\xi)^2+x_2^2]^2}d\xi - \frac{1}{\pi}\int\limits_{-a}^{a}\phi_2(\xi)\frac{(x_1-\xi)[(x_1-\xi)^2+3x_2^2]}{[(x_1-\xi)^2+x_2^2]^2}d\xi, \tag{4.2}$$

where $x_1 = x_1^{(0)}$, $x_2 = x_2^{(0)}$,

$$\phi_j(\xi) = \frac{1}{\pi\sqrt{a^2-\xi^2}}\int\limits_{-a}^{a}\frac{\sqrt{a^2-\tau^2}p_j(\tau)}{\tau-\xi}d\tau, \tag{4.3}$$

and p_1, p_2 are the components of the tractions applied on $M^{\pm}$ (see (2.10)).

2. The vector-field $\mathbf{v}$ does not necessarily satisfy the traction boundary conditions (2.10) on m_ε, and the error is to be removed by the boundary layer $\varepsilon\mathbf{w}(\boldsymbol{\zeta}, f)$. Let $m = \varepsilon^{-1}m_\varepsilon$. The vector-function $\mathbf{w}$ satisfies the homogeneous equilibrium equations (2.1) (with $\mathbf{x}$ being replaced by $\boldsymbol{\zeta}$), and the traction boundary conditions on the faces of the scaled crack m:

$$-\sin\beta\begin{pmatrix}\sigma_{11}(\mathbf{w};\boldsymbol{\zeta})\\ \sigma_{12}(\mathbf{w};\boldsymbol{\zeta})\end{pmatrix} + \cos\beta\begin{pmatrix}\sigma_{12}(\mathbf{w};\boldsymbol{\zeta})\\ \sigma_{22}(\mathbf{w};\boldsymbol{\zeta})\end{pmatrix} = \mathbf{p}^{(1)}, \tag{4.4}$$

where

$$\mathbf{p}^{(1)} = \mathbf{p} + \sin\beta\begin{pmatrix}\sigma_{11}(\mathbf{v};\mathbf{x}^{(0)})\\ \sigma_{12}(\mathbf{v};\mathbf{x}^{(0)})\end{pmatrix} - \cos\beta\begin{pmatrix}\sigma_{12}(\mathbf{v};\mathbf{x}^{(0)})\\ \sigma_{22}(\mathbf{v};\mathbf{x}^{(0)})\end{pmatrix}. \tag{4.5}$$

The solution $\mathbf{w}$ is sought in the class of functions which decay at infinity (we note that the right-hand side (4.4) is self-balanced, i.e. its principal force and moment vectors are equal to zero). The functions p_1°, p_2° that are involved in the boundary conditions (3.5) are expressed through the quantities (4.2) as follows

$$p_1^{\circ} = p_1 - \frac{\sin 2\beta}{2}(\sigma^{\circ}_{11} - \sigma^{\circ}_{22}) + \cos 2\beta\sigma^{\circ}_{12},$$

$$p_2^{\circ} = p_2 + \sin^2\beta\sigma^{\circ}_{11} + \cos^2\beta\sigma^{\circ}_{22} - \sin 2\beta\sigma^{\circ}_{12}. \tag{4.6}$$

The asymptotic representation at infinity involves the dipole matrix $\mathbf{P}$ defined in (3.4); the stress components are given by asymptotic formulae (3.6), (3.7), where r should be replaced by $|\boldsymbol{\zeta}|$.

3. The field $\varepsilon\mathbf{w}(\boldsymbol{\zeta}; f)$ produces an error of order $O(\varepsilon^2)$ in the traction boundary conditions on the faces $M^{\pm}$ of the crack M. Here, at the third step of the algorithm we introduce the function $\varepsilon^2\mathbf{q}$, which satisfies the equilibrium system (2.1) in $\mathbb{R}^2\setminus M$ and the following boundary conditions on $M^{\pm}$:

$$\sigma_{j2}(\mathbf{q}) = -F_j(x_1), \quad -a < x_1 < a \quad (j = 1, 2), \tag{4.7}$$

where the right-hand side is defined through the first term in (3.6), namely

$$F_1(x_1) = \frac{1}{2}\sin 2\beta[\Sigma_{11}(x_1', x_2') - \Sigma_{22}(x_1', x_2')] + \cos 2\beta\Sigma_{12}(x_1', x_2'),$$

$$F_2(x_1) = \sin^2\beta\Sigma_{11}(x_1', x_2') + \cos^2\beta\Sigma_{22}(x_1', x_2') + \sin 2\beta\Sigma_{12}(x_1', x_2'), \tag{4.8}$$

and

$$x_1' = \cos\beta(x_1 - x_1^{(0)}) - \sin\beta x_2^{(0)},$$

$$x_2' = -\sin\beta(x_1 - x_1^{(0)}) - \cos\beta x_2^{(0)}.$$

4. The stress-intensity factors $K_j^{\pm}$ characterising singular stress fields in the vicinity of the end points $(\pm a, 0)$ of the crack M can be evaluated as follows:

$$K_j^{\pm} = K_j^{\pm}(\mathbf{v}) + \varepsilon^2 K_j^{\pm}(\mathbf{q}) + O(\varepsilon^3), \quad j = I, II. \tag{4.9}$$

Here

$$K_I^{\pm}(\mathbf{q}) = -\frac{1}{\sqrt{\pi a}} \int_{-a}^{a} \sigma_{22}(\mathbf{q}) \left(\frac{a+t}{a-t}\right)^{\pm 1/2} dt,$$

$$K_{II}^{\pm}(\mathbf{q}) = -\frac{1}{\sqrt{\pi a}} \int_{-a}^{a} \sigma_{12}(\mathbf{q}) \left(\frac{a+t}{a-t}\right)^{\pm 1/2} dt, \tag{4.10}$$

As $x_1 \to \pm a \pm 0$ and $x_2 = 0$, the traction components σ_{12}, σ_{22} are characterized by the asymptotic formulae

$$\sigma_{12} = \frac{K_{II}^{\pm}}{\sqrt{2\pi |x_1 \mp a|}} + O(1),$$

$$\sigma_{22} = \frac{K_I^{\pm}}{\sqrt{2\pi |x_1 \mp a|}} + O(1). \tag{4.11}$$

Remark. If M is a semi-infinite crack, i.e.

$$M = \{\mathbf{x} : \ x_2 = 0, \ x_1 < l\},$$

then one can also use the results of Movchan et al (1991) and Valentini et al (1999) to evaluate the perturbation of the crack trajectory due to interaction with the micro-crack m_ε. Then it is appropriate to replace M by

$$M_\varepsilon = \{\mathbf{x} : \ x_2 = \varepsilon^2 h(x_1), \ x_1 < l\},$$

where the function h is chosen in such a way that the stress-intensity factor K_{II} (evaluated to order $O(\varepsilon^2)$) at the end of M_ε is equal to zero. It means that M_ε "propagates" in an elastic plane with a small defect (micro-crack) being a Mode-I crack. Both, the dipole field contribution given by (4.9) and the crack deflection (see the classical article by Cotterell and Rice (1980)) contribute to the final answer for the stress-intensity factors. The crack deflection $\varepsilon^2 h$ (we refer to Valentini et al (1999)) is proved to be independent of the effective elastic moduli λ_*, μ_*, and it is given by

$$\varepsilon^2 h(l) = \frac{\varepsilon^2}{8x_2^{(0)}} \Big\{ 4 - z \Big[3 + 2z - z^2 + 2\cos 2\beta (1 + 2z)(1 - z^2)$$

$$-2 \sin 2\beta (2z - 1)(1 + z)\sqrt{1 - z^2} \Big] \Big\}, \tag{4.12}$$

where

$$z = \frac{x_1^{(0)} - l}{\sqrt{(x_2^{(0)})^2 + (x_1^{(0)} - l)^2}}.$$

We note that the crack deflection has the same form in homogenized media corresponding to lattice structure both with triangular and hexagonal cells (see (2.4) and (2.5)). Also the deflection of infinity (as $l \to +\infty$) does not depend on the orientation of the micro-crack

m_ε. The crack deflection formula (4.12) differs from the one derived for the case of the rectangular lattice (see formula (7.12)) in Antipov et al (1999)). In particular, we remark that the homogenized material with rectangular cells is orthotropic and has low resistance to shear, the crack trajectory changes, as $l \to +\infty$, for different orientations of the micro-crack m_ε.

5 Interaction of a finite crack and a micro-crack in a lattice under thermal load

It is natural to assume that the cellular structure of catalytic combustor monoliths is subjected to a temperature load. Let α_T denote the coefficient of thermal expansion, and also assume that ideal thermal contact (continuity of temperature and the heat flux) is maintained on the crack faces. We consider interaction of two cracks M and m_ε (see Section 2); the right-hand side in the boundary condition (2.10) has the form

$$\mathbf{p} = (2\mu_* + 3\lambda_*)\alpha_T T\mathbf{n}. \tag{5.1}$$

In particular, for a hexagonal lattice

$$\mathbf{p} = \mathbf{p}^{hexag} = \frac{3E}{4(1-\nu^2)}\left(f - \frac{1}{2}f^3\right)\alpha_T T\mathbf{n}, \tag{5.2}$$

and for a triangular lattice

$$\mathbf{p} = \mathbf{p}^{triang} = \frac{5E}{8(1-\nu^2)} f\alpha_T T\mathbf{n}. \tag{5.3}$$

For the sake of simplicity we assume that the temperature distribution is uniform. In the asymptotic scheme described above (see Section 4) the field $\mathbf{v}$ can be defined via the Westergaard potential

$$Z_I = \frac{z}{\sqrt{z^2 - a^2}} - 1, \tag{5.4}$$

where $z = x_1 + ix_2$. Then the stress components $\sigma_{ij}(\mathbf{v})$ are given by (Sedov 1972)

$$\begin{aligned} \sigma_{11}(\mathbf{v}) &= p[ReZ_I(z) - x_2 ImZ_I(z)], \\ \sigma_{12}(\mathbf{v}) &= -px_2\Re Z_I'(z), \\ \sigma_{22}(\mathbf{v}) &= p[ReZ_I(z) + x_2 ImZ_I'(z)]. \end{aligned} \tag{5.5}$$

The boundary layer $\varepsilon\mathbf{w}(\boldsymbol{\zeta}, f)$ (it is the second term in (4.1)) satisfies the homogeneous equilibrium system (2.1) in $\mathbb{R}^2 \setminus m$, $m = \varepsilon^{-1}m_\varepsilon$, and the traction boundary conditions (4.4), where p should be replaced by (5.2) for a hexagonal lattice or by (5.3) for a triangular lattice.

The stress-intensity factors $K_j^\pm$ for the crack M are determined by (4.9), where

$$K_{II}^\pm(\mathbf{v}) = 0, \quad K_I^\pm(\mathbf{v}) = p\sqrt{\pi a}, \quad p = ||\mathbf{p}||$$

with $\mathbf{p}$ being defined by (5.2), (5.3). The perturbation terms are given by (4.7), (4.10) and they depend on the applied temperature T, position and orientation of the micro-crack m_ε. The answers for the hexagonal and triangular lattices differ just by a scalar factor.

In the following section we present evaluation of the stress-intensity factors for different positions and orientations of the micro-crack and study the local stability of the crack M.

6 Numerical examples: evaluation of the stress-intensity factors, and the local stability analysis

The asymptotic solutions derived in the text above is used to evaluate the stress intensity factors and to study the local stability of the large crack M.

In Fig. 3 we show the perturbation terms in the representations of the normalized stress-intensity factors, and these graphs, periodic in β, show that the sign of the perturbation terms depends on the orientation and position of the micro-crack m_ε. For completeness, we also present the graphs of the perturbation terms when β is fixed and θ is varying (see Fig. 4).

In both Fig. 3 and Fig. 4 we used the normalization of the stress-intensity factors of the form $K_j^{\pm}/C$, $j = I, II$, where the constant C depends on the type of the lattice. In particular, for the triangular lattice

$$C = 5EfT\alpha_T/[8(1-\nu^2)],$$

and for the hexagonal lattice

$$C = 3E(f - f^3/2)T\alpha_T/[4(1-\nu^2)].$$

To characterize the local stability of the crack M (we say that it is locally stable if the increment of the stress-intensity factor K_I is negative, and unstable otherwise) we present Fig. 5, which shows the regions of stability on the plane (θ, β); the calculations have been performed for the case when $R/a = 3$ where $R = \sqrt{(x_1^{(0)})^2 + (x_2^{(0)})^2}$.

Inside the ellipsoidal regions in Fig. 5 we have the points of local stability, and all remaining points correspond to an unstable crack.

7 Conclusion

We have analysed a perturbation problem of the crack-defect interaction in the homogenized lattice structure. Explicit asymptotic formulae for the stress-intensity factors and for the crack deflection have been derived, and the phenomenon of local stability was studied for a macro-crack in an inhomogeneous solid. The homogenization procedure is shown to be extremely efficient for the cases of cracks which are sufficiently large compared to the size of the lattice. For small cracks we use the stress concentration concept to estimate the critical load (critical temperature) required to fracture a sample with a void. The algorithm is used to compare different types of lattice structures, and includes the cases of triangular, hexagonal and square lattices that are commonly used in design of catalytic monolith combustors.

Acknowledgements

The work was supported by the U.K. Engineering and Physical Sciences Research Council (EPSRC), Grant No GR/K76634.

Appendix: Critical temperature for a lattice with a crack

The homogenization model described in the text above assumes that the crack length is sufficiently large compared to the size of an elementary cell in the lattice. The calculations

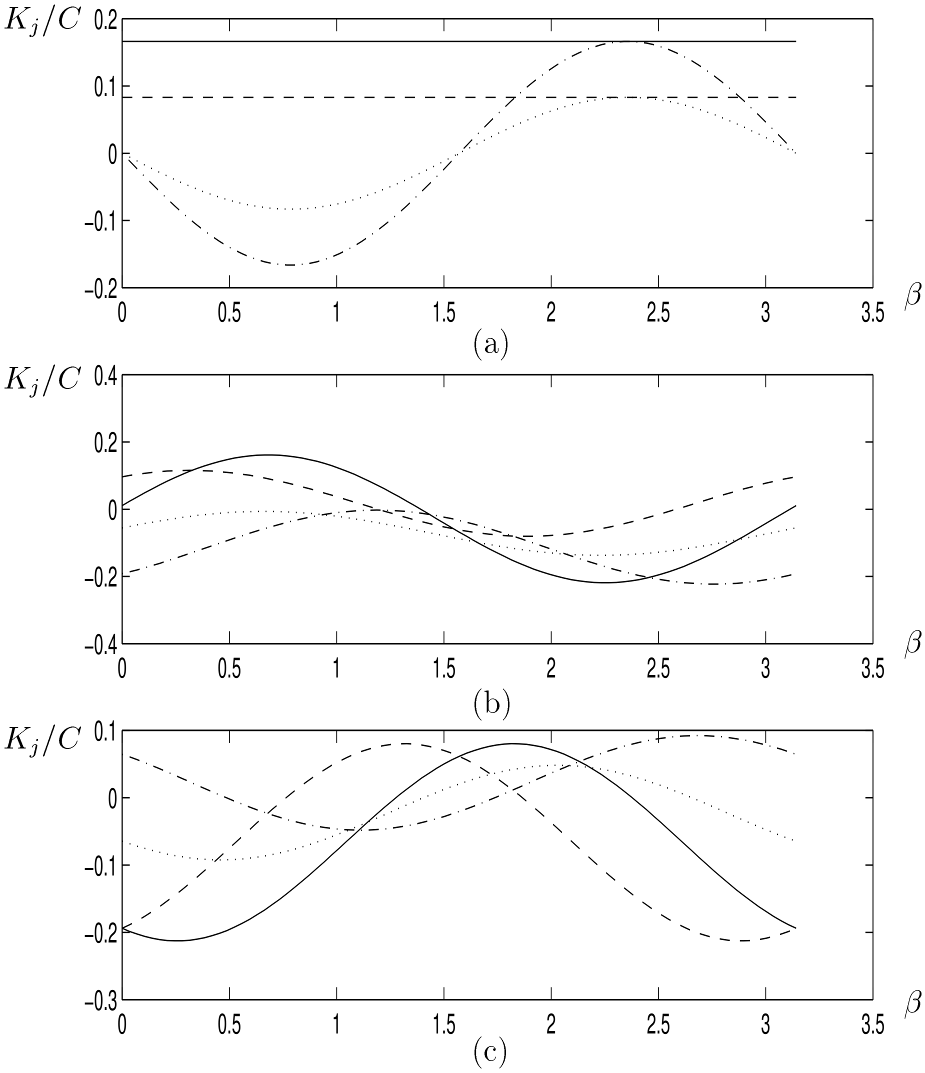

Figure 3: Perturbation of the normalized stress-intensity factors $C^{-1}K_j^{\pm}$ versus β: —— $C^{-1}K_I^{+}$; - - - $C^{-1}K_I^{-}$; $- \cdot - \cdot$ $C^{-1}K_{II}^{+}$; $\cdots$ $C^{-1}K_{II}^{-}$; (a) - $\theta = 0$; (b) - $\theta = \pi/4$; (c) - $\theta = \pi/2$.

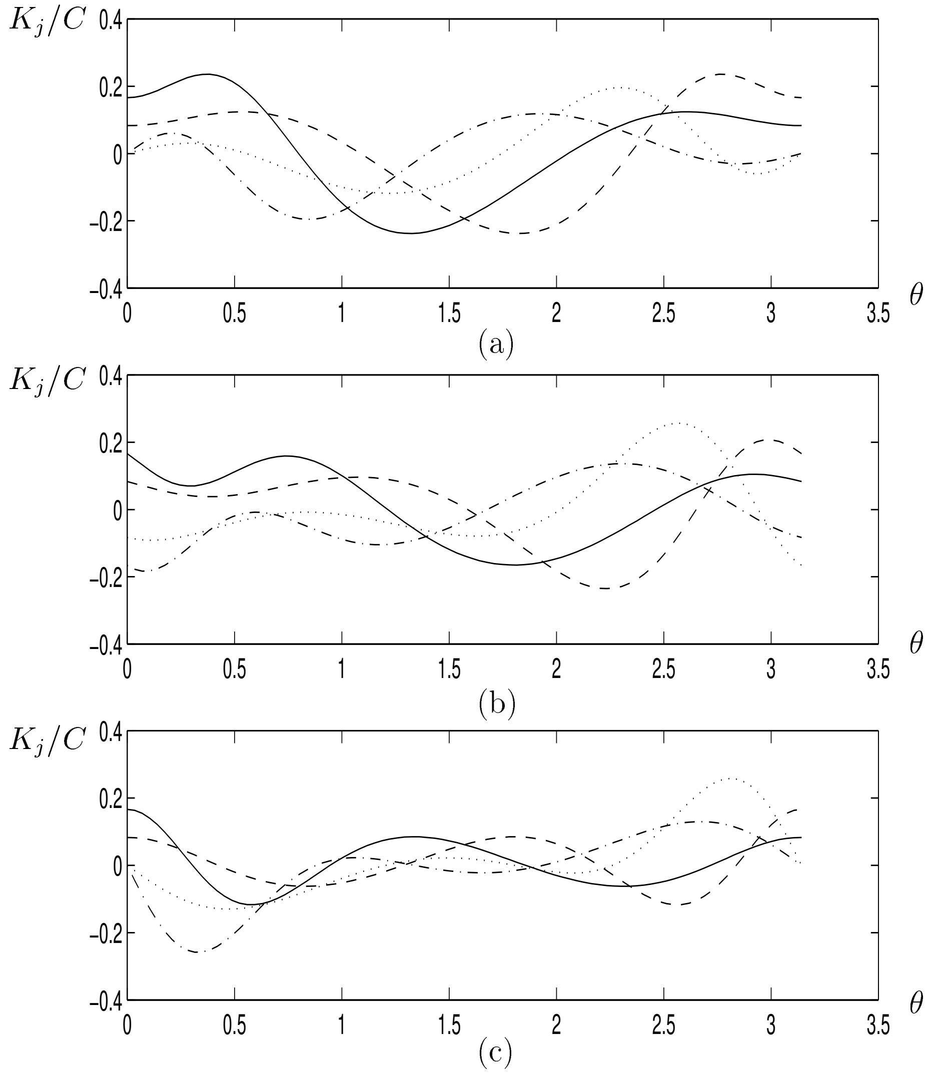

Figure 4: Perturbation of the normalized stress-intensity factors $C^{-1}K_j^{\pm}$ versus θ —— $C^{-1}K_I^+$; - - - $C^{-1}K_I^-$; $- \cdot - \cdot$ $C^{-1}K_{II}^+$; $\cdots$ $C^{-1}K_{II}^-$; (a) - $\beta = 0$; (b) - $\beta = \pi/4$; (c) - $\beta = \pi/2$.

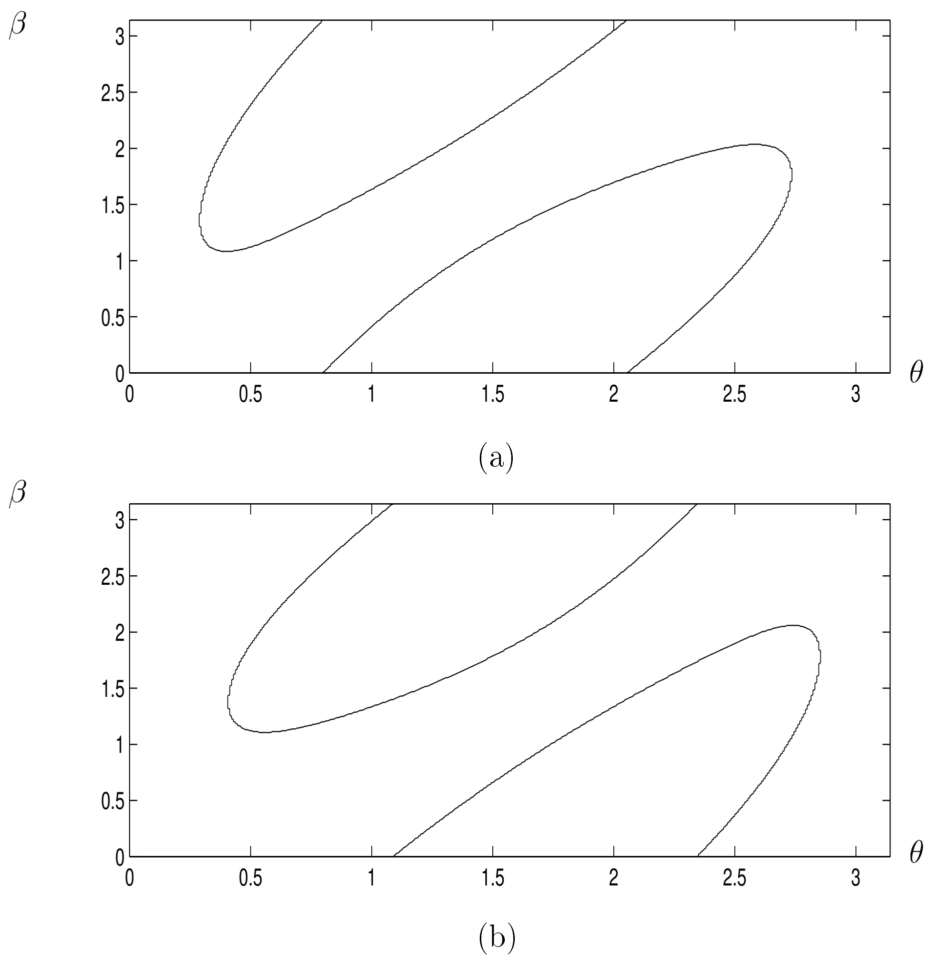

Figure 5: Regions of local stability in the plane (θ, β) for $R/a = 3$: (a) - K_I^+; (b) - K_I^-.

(a) (b)

Figure 6: The fracture test: (a) a sample without a flaw; (b) a sample with a flaw.

based on evaluation of the critical stress-intensity factor would give the lower bound of the critical temperature that causes thermal fracture of a sample. It is more appropriate for the case when the crack length is not very large to evaluate the stress concentration (rather than stress-intensity factor); it is shown that this simple approach gives reasonable agreement with the experiment.

7.1 Description of the experiment

In the experiment we used a lattice structure with square cells. Two samples were analyzed: one of the samples contained a crack, another one did not have any crack. The fracture test gave us the critical stress for undamaged lattice and a stress concentration factor associated with a crack. Both fractured samples are shown in Fig. 6.

To exclude the effect of catalyst/washcoat, experiments were performed on an uncoated ceramic monolith substrate, that was manufactured from Cordierite (2MgO.2A12O3 . 5SiO2).

The ceramic monolith, had square shaped cells, with a density of 49 cells/cm^2. Rectangular pieces were cut, that were about 6.5 cm long x 2.0 cm wide, with a thickness of 1 cm in the axial direction of the channel. Using epoxy resin, the two ends of the sample were mounted in metal brackets that were then subsequently connected to the jaws of a tensile testing machine.

The design of the jaws and the pivot on the metal brackets ensured that a uniform longitudinal force could be applied. In preliminary tests on a number of similar samples, in some of the tests the monolith fractured in proximity to the mounting bracket illustrating the presence of end effects. This was most probably caused by the distribution of epoxy in the cells used to mount the monolith in the bracket. Further tests were then performed on samples cut in the shape of the letter I. In these tests the sample broke in the narrower section (see Fig. 6(a)), and it was clear that end effects had been eliminated. Experiments were also performed on sections where 5 cells (0.5 cm) had been cut from the centre of the rectangular piece, ensuring that the fracture occurred in close proximity to the cut (see Fig. 6(b)).

The sample was then placed inside a furnace, and the temperature was raised from 50°C to 1000°C, at 50°C intervals. For each interval the sample was held at this temperature for about 20 minutes. The condition of the monolith was observed at each of these intervals. At the end of this test, it was apparent that although a readily noticeable fracture had not occurred, there was evidence of cell failure in proximity to the cuts, indicating that crack propagation was imminent.

7.2 Numerical estimates

Assume that a sample 1 has a perfect lattice structure (Fig. 6(a)), and a sample 2 has a flaw (Fig. 6(b)). Let $\sigma_c^{(j)}, j = 1, 2$, be the critical stress that causes fracture of the sample j. Also, for the sample 2 we note a stress concentration in the immediate neighbourhood of the flaw, so that at the crack extension $\sigma_{22} = \sigma_c^{(1)} = k\sigma_c^{(2)}$, where $k > 1$ stands for the stress concentration factor. Let $d = k - 1$; this quantity can be evaluated from the experiment via the simple formula

$$d = \frac{\sigma_c^{(1)} - \sigma_c^{(2)}}{\sigma_c^{(2)}}.$$

When the temperature load is applied on the crack faces, the normal stress component is specified by

$$\sigma_{22} = -\gamma T \text{ on the crack surface,}$$

where $\gamma = (2\mu_* + 3\lambda_*)\alpha_T$, α_T is the coefficient of thermal expansion, and T is temperature. The lattice structure fails when $T = T_{crit.}$ with

$$\gamma T_{crit.} d = \sigma_c^{(1)}.$$

Hence, the critical temperature $T_{crit.}$ can be evaluated in the form

$$T_{crit.} = \frac{\sigma_c^{(1)}\sigma_c^{(2)}}{\gamma(\sigma_c^{(1)} - \sigma_c^{(2)})}.$$

Taking the results of one of the test we list the set of numerical data: Young's modulus $E = 3 \times 10^{10} N/m^2$, the Poisson ratio $\nu = 0.25$, the area fraction $f = 0.2$, thermal expansion coefficient $\alpha_T = 0.75 \times 10^{-6} C^{-1}$. With $\sigma_c^{(1)}$ and $\sigma_c^{(2)}$ being defined as

$$\sigma_c^{(1)} = f_1/s_1, \quad \sigma_c^{(2)} = f_2/s_2,$$

we obtain from the experiment that the critical loads $f1$ and $f2$ have the values

$$f_1 = 187kN, \quad f_2 = 172kN,$$

and areas of cross-sections are

$$s_1 = 1.45 \times 10^{-6} m^2, \quad s_2 = 1.9 \times 10^{-6} m^2.$$

Hence, the critical temperature is evaluated as $1265^\circ C$, which is consistent with the experiment.

We remark that this simple scheme applies equally to other types of periodic structures, and it indicates the limitation of the homogenization approximation for the cases of cracks whose lengths is not very large (compared to the size of an elementary cell in the lattice).

References

Y.A.Antipov, S.T.Kolaczkowski, A.B.Movchan, A.Spence (1999), Asymptotic analysis for cracks in a catalytic monolith combustor. *Int. J. Solids Structures*, to appear.

J.Y.Chen, Y.Huang and M.Ortiz (1998), Fracture analysis of cellular materials: a strain gradient model *J. Mech. Phys. Solids*, **46**, 789-828.

B.Cotterell and J.R.Rice (1980), Slightly curved or kinked cracks. *Int. J. Fracture*, **16**, 155-169.

Gibson and Ashby (1988), Cellular Solids. Pergamon Press.

S.-X.Gong and H.Horii (1989), General solution to the problem of micro-cracks near the tip of a main crack. *J. Mech. Phys. Solids*, **37**, 27-46.

R.E.Hayes and S.T.Kolaczkowski (1997), Introduction to catalytic combustion. Gordon and Breach Publishers.

M.Hori and S.Nemat-Nasser (1987), Interacting micro-cracks near the tip in the process zone of a macro-crack. *J.Mech. Phys. Solids*, **35**, 601-629.

S.T.Kolaczkowski, P.Lin, A.B.Movchan, S.K.Serkov and A.Spence (1999), Thermal stress analysis and homogenization for catalytic combustor monoliths. *European J. of Applied Mathematics* **10**, 185-220.

A.B.Movchan S.A.Nazarov and O.R.Polyakova (1991), The quasi-static growth of a semi-infinite crack in a plane containing small defects. *C. R. Acad. Paris.,* **313**, *Serie II*, 1223-1228.

A.B.Movchan and S.K.Serkov (1997), The Polya-Szego matrices in asymptotic models of dipole composites. *European J. of Applied Mathematics* **8**, 595-621.

L.I.Sedov (1972), A course in continuum mechanics, vol.IV. Wolters-Noordhoff, Groningen.

M.Valentini, S.K.Serkov, D.Begoni and A.B.Movchan (1999) Crack propagation in a brittle elastic material with defects. *J. Appl. Mech.* **66** 79-86.